Al-Khwarizmi Engineering Journal, Vol. 6, No. 3, PP 45 - 60 (2010)

Al-Khwarizmi Engineering Journal

Free Convection in an Inclined Concentric Annular Square Cavities Filled With Porous Medium and Heated By Non-Uniform Temperature

Nabeel Mohammed Jasim
Department of Mechanical Engineering/ University of Kufa
Email: nabeelalzurfi@yahoo.com

(Received 7 April 2010; Accepted 7 September 2010)

Abstract

A numerical study of the two-dimensional steady free convection flow in an inclined annulus between two concentric square cavities filled with a porous medium is presented in this paper for the case when the side outer walls are kept with differentially heated temperature while the horizontal outer walls and the inner walls are insulated. The heated wall is assumed to have spatial sinusoidal temperature variation about a constant mean value. The Darcy model is used and the fluid is assumed to be a standard Boussinesq fluid. For the Cartesian coordinate system, the governing equations which were used in stream function form are discretized by using the finite difference method with successive under – relaxation method (SUR) and are solved by Gauss-Siedel iterative method. The upwind scheme was used for the transport terms in the energy conservation equation. The results are presented to demonstrate the streamlines, the isotherms, and the Nusselt number depending on the Rayleigh number ranging from (Ra =10 to 1000), dimension ratio from (Dr = 0.15 to 0.45), and the inclination angle from ($\varphi = 0^o$ to 45^o). Also the effects of the amplitude (ε =0 to 1) and the wave number (f =0 to 5) of the heated side wall temperature variation on the free convection are investigated. The results show the effect of previous parameters (Ra, Dr, φ , ε , and f) on the flow fields and temperature profiles. It also show that the average Nusselt number is a strong function of the Rayleigh number, inclination angle, dimension ratio, and temperature variation. The peak value of the average Nusselt number based on the hot wall temperature is observed to occur at dimension ratio of (0.15), inclination angle of (40.1°), amplitude and wave number (1 & 0.75) for Rayleigh number of (1000).

Keywords : *Free convection, inclined annulus, porous medium, sinusoidal temperature.*

1. Introduction

Convective heat transfer in fluid-saturated porous media has received considerable attention over the last few decades. This interest has been stimulated by many applications in, for example, packed sphere beds, high performance insulation for buildings, chemical catalytic reactors, grain storage, and geophysical problems such as frost heave. Porous media are also of interest in relation to the underground spread of pollutants, to solar power collectors, and to geothermal energy systems etc [1].

Natural or free convection in a porous medium has been studied extensively. Cheng [2] provides a comprehensive review of the literature on free convection in fluid saturated porous media with a focus on geothermal systems. Oosthuizen and Patrick [3] performed numerical studies of natural convection in an inclined square enclosure with part of one wall heated to a uniform temperature and with the opposite wall uniformly cooled to a lower temperature and with the remaining wall portions. The enclosure is partially filled with a fluid and partly filled with a porous medium, which is saturated with the same fluid. The main results considered were the mean heat transfer rate across the enclosure. Nithiarasu et al. [4] examined effects of applied heat transfer coefficient on the cold wall of the cavity upon flow and heat transfer inside a porous medium. The differences between the Darcy and non-Darcy

flow regime are clearly investigated for different Darcy, Rayleigh and Biot numbers and aspect ratio. Variations in Darcy, Rayleigh and Biot numbers and aspect ratio significantly affect natural flow convective pattern. Recently, Al-Amiri [5] performed numerical studies of momentum and energy transfer in a lid-driven cavity filled with a saturated porous medium. In this study, the force convection is induced by sliding the top constant-temperature wall. It was found that the increase in Darcy number induces flow activities causing an increase in the fraction of energy transport by means of convection. With similar description of the domain configuration. Nawaf [6] performed numerical study of the two-dimensional unsteady natural convection flow in a square cavity filled with a porous medium and with sidewall heating. The temperature of the hot sidewall oscillates in time about a constant value while the cold wall is held at a constant temperature; the horizontal walls are adiabatic. It was concluded that the Nusselt number becomes negative over part of the period for Rayleigh number 10^3. Caltagirone and Bories [7] studied the stability criteria of free convective flow in an inclined porous layer. Vasseur et al. [8] investigated the natural convection in a thin inclined porous layer exposed to a constant heat flux and in other contributions by Sen et al. [9] and Baytas [10]. The aforementioned natural convection is only related to buoyancy-driven flows. Previous investigations have merely focused on momentum and energy transfer in cavity filled with a saturated porous medium subjected to prescribed temperature and prescribed wall heat flux conditions. However, only a very limited amount of numerical work on momentum and energy transfer in a square porous cavity where the cavity walls are subjected to temperature variation has been reported. The only study reported so far for this case is by Saeid et al.[11] and Yoo [12]. They obtained numerical results for this problem at low Rayleigh numbers.

The brief literature review shows that there are no studies of free convection in the geometry of present study heated with spatial sinusoidal temperature variation. Thus, the aim of this work is to study numerically the problem of steady free convection in an inclined annulus between two concentric square cavities filled with a porous medium, using the Darcy model, when one of its vertical outer walls is heated with spatial sinusoidal temperature variation about a constant mean value and the other wall is suddenly cooled, while the horizontal outer walls and the inner walls are insulated. The influences of associated parameters such as heat transfer coefficient, Rayleigh number (Ra = 10 – 1000), inclination angle ($\varphi = 0^o - 45^o$), dimension ratio (Dr = 0.15 – 0.45), amplitude ($\varepsilon = 0 - 1$) and wave number (f = 0 – 5) on the flow and thermal configurations were examined. To give good indication about the influence of system parameters, results were formulated using modern techniques and presented in details using Excel and Surfer software. This work is done by solving the governing equations that represent the problem numerically using a finite difference scheme.

2. Mathematical Model

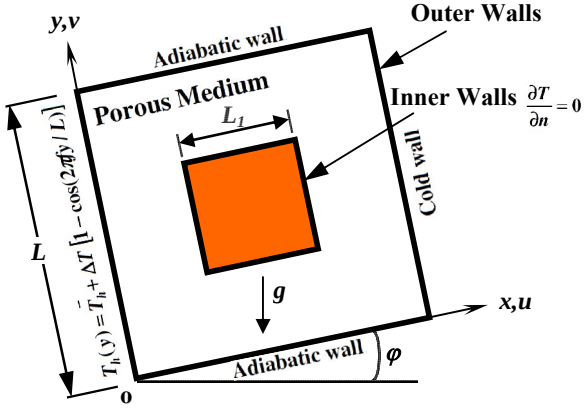

Fig.1. Problem Geometry and Coordinate System.

The physical configuration and coordinate system of the problem under consideration are depicted in Fig. (1). The inclined annulus between two concentric square cavities is filled with a fluid – saturated porous medium. Angle of inclination of geometry measured from horizontal plane to the adiabatic wall of the geometry. It is assumed that the left vertical outer wall is heated with spatial sinusoidal temperature variation about a constant mean value and the right vertical outer wall is held at a constant temperature (T_c), while the other walls are adiabatic. All walls of the cavities are further assumed to be impermeable. In the porous medium, Darcy's law is assumed to hold, and the fluid is assumed to be a normal Boussinesq fluid. The viscous drag and inertial terms in the equation of motion are neglected. With these assumptions, the dimensional governing equations as continuity, momentum and energy in an isotropic and homogeneous porous medium can be written as follows [1]:

$$\frac{\partial u}{\partial x}+\frac{\partial v}{\partial y}=0 \qquad \ldots(1)$$

$$\frac{\partial p}{\partial x}+\rho g\sin\varphi+\frac{\mu}{K}u=0 \qquad \ldots(2)$$

$$\frac{\partial p}{\partial y}+\rho g\cos\varphi+\frac{\mu}{K}v=0 \qquad \ldots(3)$$

The momentum equation is differential by based on Darcy's law of flow, which is:

$$\frac{\partial u}{\partial y}-\frac{\partial v}{\partial x}=-\frac{\rho_o g\beta K}{\mu}\left(\frac{\partial T}{\partial x}\cos\varphi-\frac{\partial T}{\partial y}\sin\varphi\right) \ldots(4)$$

$$u\frac{\partial T}{\partial x}+v\frac{\partial T}{\partial y}=\alpha\left(\frac{\partial^2 T}{\partial x^2}+\frac{\partial^2 T}{\partial y^2}\right) \qquad \ldots(5)$$

where u and v are the velocity components along x and y axes, T is the fluid temperature. The physical meanings of the other quantities are given in the Nomenclature. It is assumed that the temperature of the hot wall has a sinusoidal variation about a constant mean value in the form[12] :

$$T_h(y)=\bar{T}_h+\Delta T\left[1-\cos(2\pi fy/L)\right] \qquad \ldots(6)$$

where ΔT and f denote, respectively, the amplitude and wave number of the oscillating hot wall temperature. The temperature of the hot wall is remaining higher than cold wall temperature. Equations (4 & 5) are subject to the following boundary conditions at the inner and outer walls :

a) *For the outer walls :*

$$u(0,y)=v(0,y)=0,\quad T(0,y)=T_h(y) \qquad \ldots(7a)$$
$$u(L,y)=v(L,y)=0,\quad T(L,y)=T_c \qquad \ldots(7b)$$
$$u(x,0)=v(x,0)=0,\quad \partial T(x,0)/\partial y=0 \qquad \ldots(7c)$$
$$u(x,L)=v(x,L)=0,\quad \partial T(x,L)/\partial y=0 \qquad \ldots(7d)$$

b) *For the inner walls* :

$$u=v=0,\quad \partial T/\partial n=0 \qquad \ldots(7e)$$

where (*n*) is the normal direction on the wall.
The above equations are written in terms of the stream function defined as :

$$u=\frac{\partial\psi}{\partial y},\qquad v=-\frac{\partial\psi}{\partial x} \qquad \ldots(8)$$

The Eqs. (1-3) can be written in non – dimensional form as follows :

$$\frac{\partial^2\psi}{\partial X^2}+\frac{\partial^2\psi}{\partial Y^2}=-Ra\left[\frac{\partial\theta}{\partial X}\cos\varphi-\frac{\partial\theta}{\partial Y}\sin\varphi\right] \ldots(9)$$

$$\frac{\partial\psi}{\partial Y}\frac{\partial\theta}{\partial X}-\frac{\partial\psi}{\partial X}\frac{\partial\theta}{\partial Y}=\frac{\partial^2\theta}{\partial X^2}+\frac{\partial^2\theta}{\partial Y^2} \qquad \ldots(10)$$

The non – dimensional parameters are listed as :

$$X=\frac{x}{L},\quad Y=\frac{y}{L},\quad \theta=\frac{T-T_o}{T_h-T_c},\quad \psi=\frac{\psi}{\alpha},$$

$$Dr=\frac{L_1}{L},\qquad Ra=\frac{\rho_o g\beta K(\bar{T}_h-T_c)L}{\mu\alpha} \qquad \ldots(11)$$

where $T_o=(T_h+T_c)/2$, Ra is the Rayleigh number, Dr is the dimension ratio or dimensional width or height of the inner wall, and the boundary conditions (7) become :

a) For the outer walls :

$$\psi(0,Y)=0,\quad \theta(0,Y)=0.5+\varepsilon\left[1-\cos(2\pi fY)\right] \ldots(12a)$$
$$\psi(1,Y)=0,\quad \theta(1,Y)=-0.5 \qquad \ldots(12b)$$
$$\psi(X,0)=0,\quad \partial\theta(X,0)/\partial Y=0 \qquad \ldots(12c)$$
$$\psi(X,1)=0,\quad \partial\theta(X,1)/\partial Y=0 \qquad \ldots(12d)$$

b) For the inner walls :

$\psi=0,\quad \partial\theta/\partial n=0$ on the whole inner walls boundary (represented by Dr) …(12e)

where $\varepsilon=\Delta T/(\bar{T}_h-T_c)$ is the non-dimensional amplitude of the hot wall temperature oscillation.

Now, the local and mean Nusselt numbers are calculated via Eqs. (13a) and (13b), respectively.

$$Nu=\left(-\frac{\partial\theta}{\partial X}\right)_{X=0} \qquad \ldots(13a)$$

$$Nua=-\int_0^1 Nu\,dY \qquad \ldots(13b)$$

Equation (13b) is obtained by using Simpson's rule.

3. Numerical Method

For the solution of governing equations (9 & 10) are subject to their corresponding boundary conditions given in Eq.(12). A finite-difference technique has been used. The solution domain, therefore, consists of grid points at which the discretized equations are applied. In this domain X and Y vary from 0 to 1. Uniform grids in X and Y directions were used for all computations. Using the central – difference finite difference method at the representative interior point (i,j), Eq.(9) may be written as [13] :

$$\psi_{i,j} = ((\psi_{i+1,j} + \psi_{i-1,j})\Delta Y^2 + (\psi_{i,j+1} + \psi_{i,j-1})\Delta X^2 + 0.5\Delta Y^2.\Delta X.Ra(\theta_{i+1,j} - \theta_{i-1,j})\cos\varphi - 0.5\Delta Y.\Delta X^2 .Ra(\theta_{i,j+1} - \theta_{i,j-1})\sin\varphi)/(2\Delta X^2 + 2\Delta Y^2) \quad \ldots(14)$$

Also, The energy equation (Eq. (10)) may be written as :

$$\frac{A1}{2\Delta X}\frac{\partial\theta}{\partial Y} - \frac{A2}{2\Delta Y}\frac{\partial\theta}{\partial X} + \frac{\theta_{i+1,j} - 2\theta_{i,j} + \theta_{i-1,j}}{\Delta X^2} + \frac{\theta_{i,j+1} - 2\theta_{i,j} + \theta_{i,j-1}}{\Delta Y^2} = 0 \quad \ldots(15)$$

The upwind scheme was used for the transport terms in the energy conservation equation. This technique can be introduced to maintain the diagonal dominance coefficient of ($\theta_{i,j}$) in Eq.(10) which determines the main diagonal element of the resulting linear system. This technique is outlined as follows [14] :
set :

$$A_1 = \psi_{i+1,j} - \psi_{i-1,j} \quad \ldots(16a)$$

$$A_2 = \psi_{i,j+1} - \psi_{i,j-1} \quad \ldots(16b)$$

Now, if :

$$A1 \geq 0,\ \frac{\partial\theta}{\partial Y} = \frac{\theta_{i,j+1} - \theta_{i,j}}{\Delta Y} \quad \ldots(17a)$$

$$A1 < 0,\ \frac{\partial\theta}{\partial Y} = \frac{\theta_{i,j} - \theta_{i,j-1}}{\Delta Y} \quad \ldots(17b)$$

And, If :

$$A2 \geq 0,\ \frac{\partial\theta}{\partial X} = \frac{\theta_{i,j} - \theta_{i-1,j}}{\Delta X} \quad \ldots(18a)$$

$$A2 < 0,\ \frac{\partial\theta}{\partial X} = \frac{\theta_{i+1,j} - \theta_{i,j}}{\Delta X} \quad \ldots(18b)$$

To assure the diagonal dominance of the coefficient matrix for ($\theta_{i,j}$), which depends on the sign of (A1) and (A2), Eq. (10) is expressed in the following difference forms :

$$\theta_{i,j} = (1 - Fs)\,\theta_{i,j}^{old} + Fs.(\Delta Y^2\,\theta_{i+1,j} + (\Delta Y^2 + (\Delta X.\Delta Y .A2)/2)\,\theta_{i-1,j} + (\Delta X^2 + (\Delta X.\Delta Y.A1)/2)\,\theta_{i,j+1} + \Delta X^2 .\theta_{i,j-1})/(2(\Delta X^2 + \Delta Y^2) + (\Delta X.\Delta Y/2)(A1 + A2))$$

For $A1 \geq 0$ and $A2 \geq 0$ …(19)

$$\theta_{i,j} = (1 - Fs)\,\theta_{i,j}^{old} + Fs.((\Delta Y^2 - (\Delta X.\Delta Y.A2)/2)\,\theta_{i+1,j} + \Delta Y^2\,\theta_{i-1,j} + (\Delta X^2 + (\Delta X.\Delta Y.A1)/2)\,\theta_{i,j+1} + \Delta X^2 .\theta_{i,j-1})/(2(\Delta X^2 + \Delta Y^2) + (\Delta X.\Delta Y/2)(A1 - A2))$$

For $A1 \geq 0$ and $A2 < 0$ …(20)

$$\theta_{i,j} = (1 - Fs)\,\theta_{i,j}^{old} + Fs.((\Delta Y^2 - (\Delta X.\Delta Y.A2)/2)\,\theta_{i+1,j} + \Delta Y^2\,\theta_{i-1,j} + \Delta X^2\,\theta_{i,j+1} + (\Delta X^2 - (\Delta X.\Delta Y.A1)/2) .\theta_{i,j-1})/(2(\Delta X^2 + \Delta Y^2) - (\Delta X.\Delta Y/2)(A1 + A2))$$

For $A1 < 0$ and $A2 < 0$ …(22)

The solution in the above linear algebraic equation was performed using Successive Under Relaxation (SUR) method [14] (represented by factor Fs, as shown in Eqs. (19 – 22)) to accelerate the convergence of Eq. (10); value of (0.6) was taken for under relaxation parameter (Fs).

Also, a one – sided finite – difference expression is used for the derivative at the boundary [15], as follows (see Fig. 2):

$$\left(\frac{\partial\phi}{\partial x}\right)_1 = \frac{-3\phi_1 + 4\phi_2 - \phi_3}{2\Delta x} \quad \ldots(23)$$

A converged solution was obtained by iterating in time until variations in the primitive variables between subsequent time steps were [14 & 15] :

$$\sum\left|\frac{\phi_{i,j}^{n+1} - \phi_{i,j}^{n}}{\phi_{i,j}^{n+1}}\right| < 10^{-6} \quad \ldots(24)$$

where ϕ stands for ψ and θ, and n denotes the number of iterations.

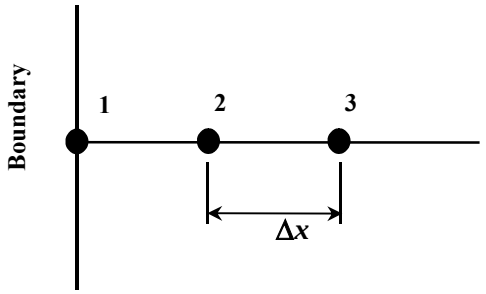

Fig. 2. One Side of the Grid Point at the Boundary.

4. Grid Independence and Validation Study

Grid independence study has been performed for grid sizes from (40×40) to (100×100) and presented in Table 1. A grid size of (80×80) has been found to be appropriate with less than (0.25 %) for the average Nusselt number when compared to the next grid size of (100×100).

To show the validation of the present numerical results, the numerical algorithm used in this study was tested with the classical natural convection heat transfer problem in a rectangular porous cavity using the same boundary conditions. To compare the present numerical results with those of natural convection in rectangular domain subjected to different uniform temperature on its horizontal walls with the left and right sides are insulated. The inclination angle, the dimension ratio, and the amplitude and the wave number is set to zero. The validation results are presented in Table 2. We see that the percentage deviation in the average Nusselt number values is from (2.5 % to 3.22 %).

Table 1,
Grid independence Study Results with Ra=10 and 100, Dr = 0.15, 0.3 and 0.45 for f =0, ε =0, and φ=0.

Ra		Values of average Nusselt number			
		Grid size			
		40×40	60×60	80×80	100×100
10	Dr = 0.15	0.9688	0.9824	0.9727	0.9724
	Dr = 0.3	0.8352	0.8379	0.8385	0.8386
	Dr = 0.45	0.6547	0.6790	0.6711	0.6708
100	Dr = 0.15	1.848	1.970	1.979	1.984
	Dr = 0.3	1.277	1.321	1.343	1.346
	Dr = 0.45	0.8103	0.8876	0.8921	0.8924

Table 2,
Average Nusselt Number Comparison for the Rectangular Porous Layers and present Work at Dr = 0, f =0, ε =0, and φ=0.

Ra	Values of average Nusselt number				
	Chan et al [16]	Burns et al. [17]	Bejan & Tien [18]	Present work	Error max. (± %)
50	2.1	2.2	---	2.17	3.22
100	3.56	3.6	3.6	3.51	2.5

5. Results and Discussion

A numerical analysis was performed to obtain free convection heat transfer and fluid flow in an inclined annulus between two concentric square cavities filled with a porous medium, with parameters of Rayleigh number (Ra), dimension ratio (Dr), amplitude and wave number (ε & f), and the inclination angle (φ).

5.1. Effects of amplitude (ε) and wave number (f)

Figs. (3 to 6) show the contour lines of flow fields and the temperature distribution at (Ra = 10 and 1000) for different values of amplitude (ε = 0, 0.2, 0.6, and 1). The above figures show the effect of Rayleigh number and amplitude on flow fields and temperature distribution for different values of dimension ratio (Dr= 0.15, 0.3,

and 0.45) at f = 1 and φ=0. Figs. (3a and 5a) indicate that the flow consists of a two rotating vortex. The rotating vortex turns in clockwise and is located at top and lower regions of inner walls. It is clearly shown that when the amplitude (ε) increases for Ra > 100, the numbers of rotating vortex are increased to three cells, the small one is in counterclockwise and is locate at the left top corner of the annulus, which can be seen in Fig. (5 c and d). As Rayleigh number (Ra) increases, the location of rotating vortex is changed and is locate at the right and left side of inner walls; see Figs. (3a and 5a). The flow shows jet – like behavior between the inner and outer walls and a small eddies were formed on the left top corner of the annulus due to high velocity. The isotherms are shown in Figs.(4 and 6). For low Rayleigh number ($Ra \leq 100$), the isotherms are almost parallel to side walls due to dominance of conduction mechanism, as shown in Fig. (4a). As Ra or ε increases, Producing closer streamlines near the walls and change the direction of the isotherms, as shown in Fig. (4 b,c, and d) and Fig. (5). Fig. (5 b) shows a rest point on left top side of annulus at low values of ε, while the values of $\varepsilon > 0.2$, producing a wavy streamlines (Fig. 9 a & b). But this behavior does not continue for high values of ε, where a secondary flow producing in this region (Fig. 9 c). As ε is increased further for given values of Ra, the streamlines become closer to the walls producing strong boundary layer effects on the side walls. As a result, the stratified region becomes bigger, as shown in Figs. (4 & 6 b, c, and d). It is also noticed that from above figures the temperature gradient is positive in the left top corner of annulus which leads to negative values of Nusselt number as shown in Fig. (12). Figs. (7 to 10) show the contour lines of flow fields and the temperature distribution at (Ra = 10 and 1000) for same previous values of amplitude but at wave numbers (f = 5). It is noticed that from the temperature distribution on left side wall (hot wall), the direction of the isotherms changes from negative to positive values which leads to change the value of local Nusselt number as a sinusoidal function from positive to negative on the wall (Fig. 11). The effect of wave number (f) on the distributions of local Nusselt number for cold and hot walls at Ra = 1000, Dr= 0.3, φ= 0, and ε= 0.6 is shown in Fig. (11). It is clear that the local Nusselt number along the cold wall has a peak value at f = 0.75. While the local Nusselt number along the hot wall is changed by sinusoidal function according to the values of (f). The value of local Nusselt number becomes negative at high values of wave number (f =5). This negative value of local Nusselt number occurs at upper portion of the hot wall owing to returning some amount of the energy rejected from the bottom of hot wall to the same wall (hot wall) at upper part. Fig. (14) represents the distribution of local Nusselt number on cold and hot walls with different values of amplitude (ε) at Ra = 1000, Dr= 0.3, φ= 0, and f = 1. As ε is increased, the value of local Nusselt number is increased along the hot and cold walls, while the upper part of hot wall has a negative values of local Nusselt number. Figs.(15 and 16) represent the distribution of local Nusselt number on cold and hot walls with different values of Rayleigh number (Ra = 10, 100, and 200) at ε= 0.6, Dr= 0.3, φ= 0, and f = 1 & 3. It is seen that the local Nusselt number increases as Ra increases expressing the existence and increase of convective heat transfer. Fig. (18) represents the variation of average Nusselt number for hot wall with different values of amplitude and wave number at $\varphi = 30^{o}$ and Ra= 10 & 1000. It is found that the Nusselt number increases as (f) increases and reaches the peak value at f = 0.75 for a given value of ε, then the value of Nusselt number deceases from its peak value as (f) increases more. Also It is seen that the effect of ε on Nusselt number is more pronounced as the Ra number increase for a given values of f.

5.2. Effects of dimension ratio (Dr)

In order to study the effect of the dimension ratio (Dr) on the heat and fluid flow, three different values are considered: 0.15, 0.3, and 0.45. Figs. (3 to 6) show the contour lines of flow fields and the temperature distribution for different values of dimension ratio (Dr) at Ra= 10 and 1000. As seen in Figs. (3 & 5) , the form of the streamlines is affected by the increasing value of the dimension ratio. Also, the temperature profiles are affected by the dimension ratio (Dr) as shown in Figs.(4 & 6). Decreasing Dr intensifies the temperature profiles near the outer wall where the convection becomes stronger due to increasing the space between the side outer walls when Dr decreases. As the heat transferred from outer walls is increased, the thermal boundary layers near the outer wall become thinner with the decreasing Dr, while those near the inner wall become thicker. Accordingly, as will be shown later, this will affect the heat transfer rates. Fig.(12) represents the distribution of local Nusselt number on cold and hot walls with different values of dimension ratio (Dr = 0.15, 0.3, and 0.45) at Ra = 1000,

$\varepsilon = 0.6$, $\varphi = 0$, and $f = 1$. Increasing the dimension ratio (Dr) (from 0 – 0.45) decreases the local Nusselt number along the hot and cold walls by (10 – 30 %) due to increasing the area of inner cavity (represented by Dr) which leads to obstruct the heat transfer from hot to cold wall. The local Nusselt number is changed by sinusoidal function along the hot wall.. Fig. (17) shows the variation of average Nusselt number for the hot wall as a function of (Dr and Ra). As shown, an increase at (Dr) leads to a decrease of (Nua) for a given value of (Ra).

5.3. Effects of inclination angle (φ)

In order to examine the effects of inclination angle (φ), computations are carried out for a fluid with the inclined angle (φ) varying from (0^o to 45^o). Figs. (7 to 10) show the effect of inclination angle (φ) on the flow fields and the temperature distribution at Ra = 1000. The streamlines and temperature distribution are symmetric with respect to the diagonal of annulus for ($\varphi = 0$ & $\varepsilon = 0$, Fig. 3a), while this symmetry does not occur for the other values of (φ). Moreover, for all the considered cases, the dimensionless temperature field shows that the lower part of the annulus is almost isothermal with a temperature close to the wall temperature and that the highest temperature gradients occur in the side parts of the annulus. In figs. (7 & 9), the streamlines are plotted for (Ra = 1000, $\varepsilon = 1$, and Dr = 0.15 & 0.45, with $\varphi = 0^\circ$, $\varphi = 30^\circ$, and $\varphi = 45^\circ$, respectively. The above figures show two non–symmetric convective cells. The Distribution of local Nusselt number on cold and hot walls is shown in Fig. (13) with different values of inclination angle (φ) at Ra = 1000, Dr = 0.15, $f = 3$, and $\varepsilon = 0.6$. For $\varphi < 45^o$, as φ increases the value of local Nusselt number along the cold and hot walls increases and has a peak value at ($\varphi = 39^o - 41^o$). While the local Nusselt number decreases from its peak value as φ increases more for the given values of other parameters. Fig.(19) shows the variation of average Nusselt number for the hot wall as a function of (φ and Ra). At $\varepsilon = 0$, it can be seen that the Nusselt number attains the maximum value at $\varphi = 39.2^o$ because the effective height of the hot wall take the maximum value at this orientation which represents maximum heat transfer rate for named conditions; but at $\varphi = 45^o$, the effective height of the hot wall decreases due to the gravitational buoyancy force. However, there is little difference among the magnitude of the average Nusselt number at different inclination angle for $\varepsilon = 0$. When there exists temperature variation on hot wall ($\varepsilon > 0$), the heat transfer is enhanced with the increase of φ and the average Nusselt number takes maximum value at about $\varepsilon = 1$ and Dr = 0.15 for $\varphi = 40.1^o$.

6. Conclusions

A numerical study was performed to examine free convection heat transfer and fluid flow in an inclined annulus between two concentric square cavities filled with a porous medium. Important conclusions were obtained from the study as follows :

1- Heat transfer is increased with the increase of Rayleigh number.
2- The local Nusselt number on hot wall (heated wall) is changed with a sinusoidal function according to its temperature variation.
3- Average Nusselt number is changed by a sinusoidal function as a wave number (f) increases and has a maximum value (maximum heat transfer) at (f = 0.75) for high values of Rayleigh number (Ra = 500 and 1000) and at (f = 0.7) for (Ra = 10 to 200).
4- As the amplitude (ε) increases, value of Nusselt number is increased making wavy variation in streamlines.
5- Numerical results reveal that an increase at the dimension ratio (Dr) will result in a decrease at the average Nusselt number at the hot wall.
6- The rate of heat transfer is enhanced with the increase angle of inclination (φ) of the inclined annulus from horizontal plane and the peak in average Nusselt number occurs between ($39^o \le \varphi \le 41^o$), depending upon previous parameters. While the average Nusselt number decreases from its peak value as φ increases from horizontal above these values.

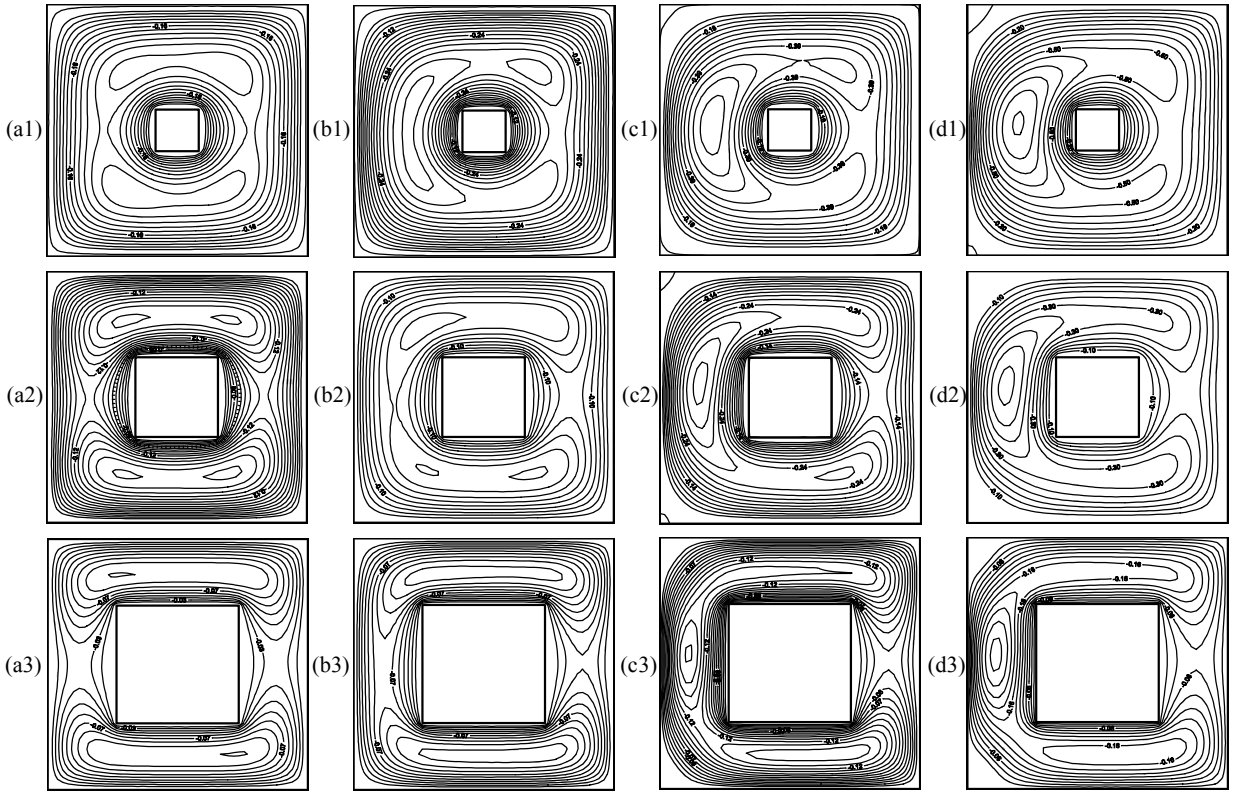

Fig. 3. Streamlines of Flow at Ra= 10, f =1, & φ=0 for a) ε = 0, b) ε = 0.2, c) ε = 0.6, d) ε = 1 and 1) Dr= 0.15, 2) Dr= 0.3, 3) Dr= 0.45 .

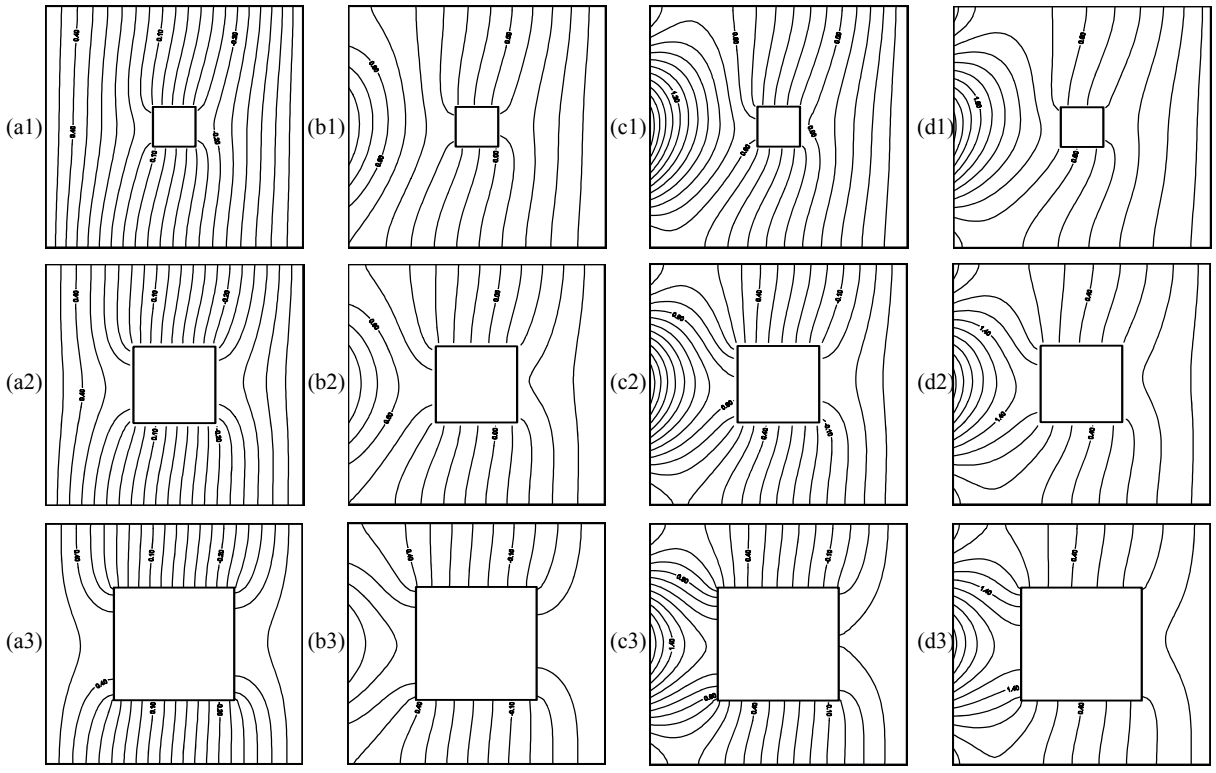

Fig.4. Isothermal Contours at Ra= 10, f =1, & φ=0 for a) ε = 0, b) ε = 0.2, c) ε = 0.6, d) ε = 1 and 1) Dr= 0.15, 2) Dr= 0.3 3) Dr= 0.45 .

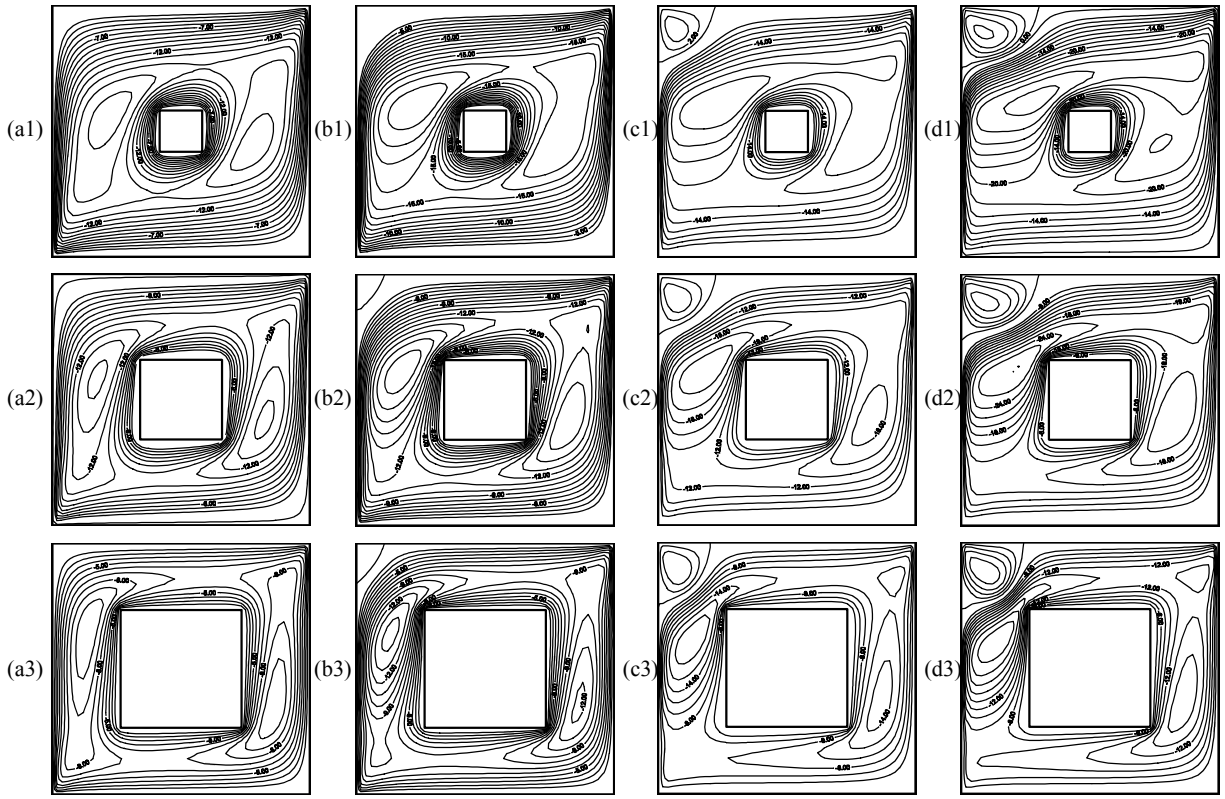

Fig. 5. Streamlines of Flow at Ra= 1000, f =1 & φ=0, for a) ε = 0, b) ε = 0.2, c) ε = 0.6, d) ε = 1 and 1) Dr= 0.15, 2) Dr= 0.3, 3) Dr= 0.45 .

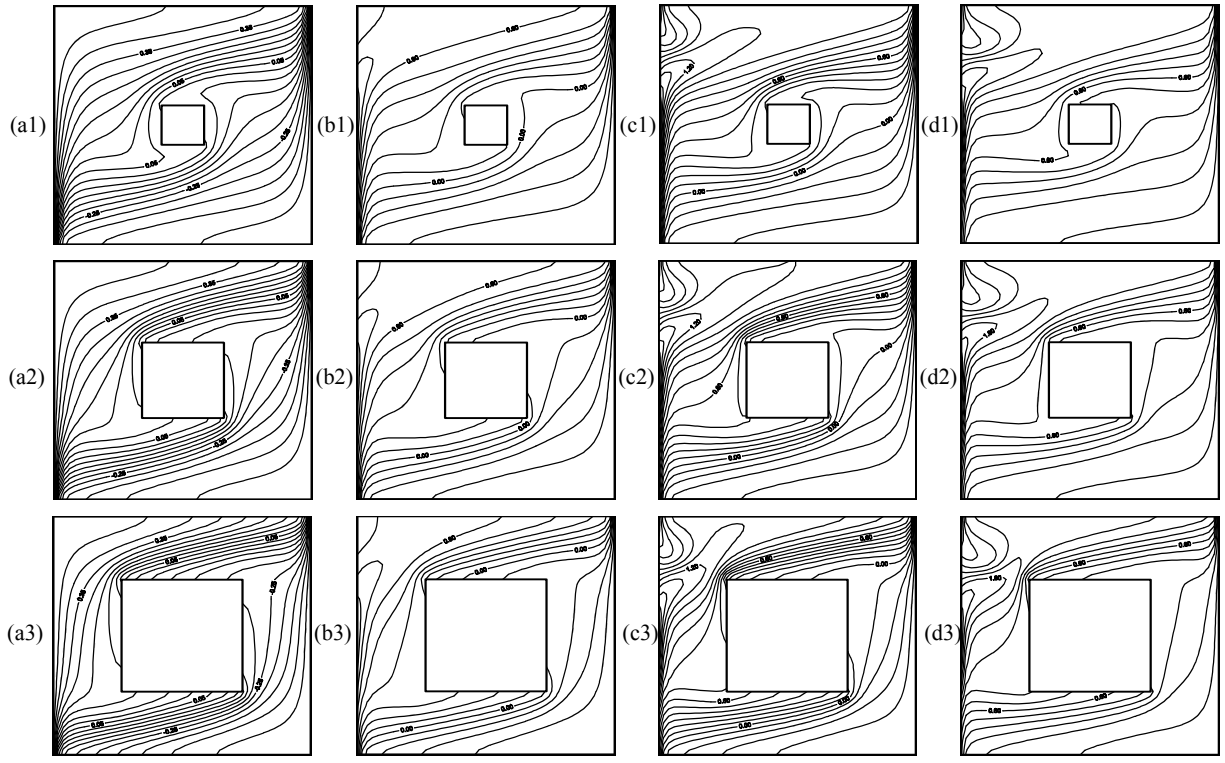

Fig. 6. Isothermal Contours at Ra= 1000, f =1 & φ=0 for a) ε = 0, b) ε = 0.2, c) ε = 0.6, d) ε = 1 and 1) Dr= 0.15, 2) Dr= 0.3, 3) Dr= 0.45 .

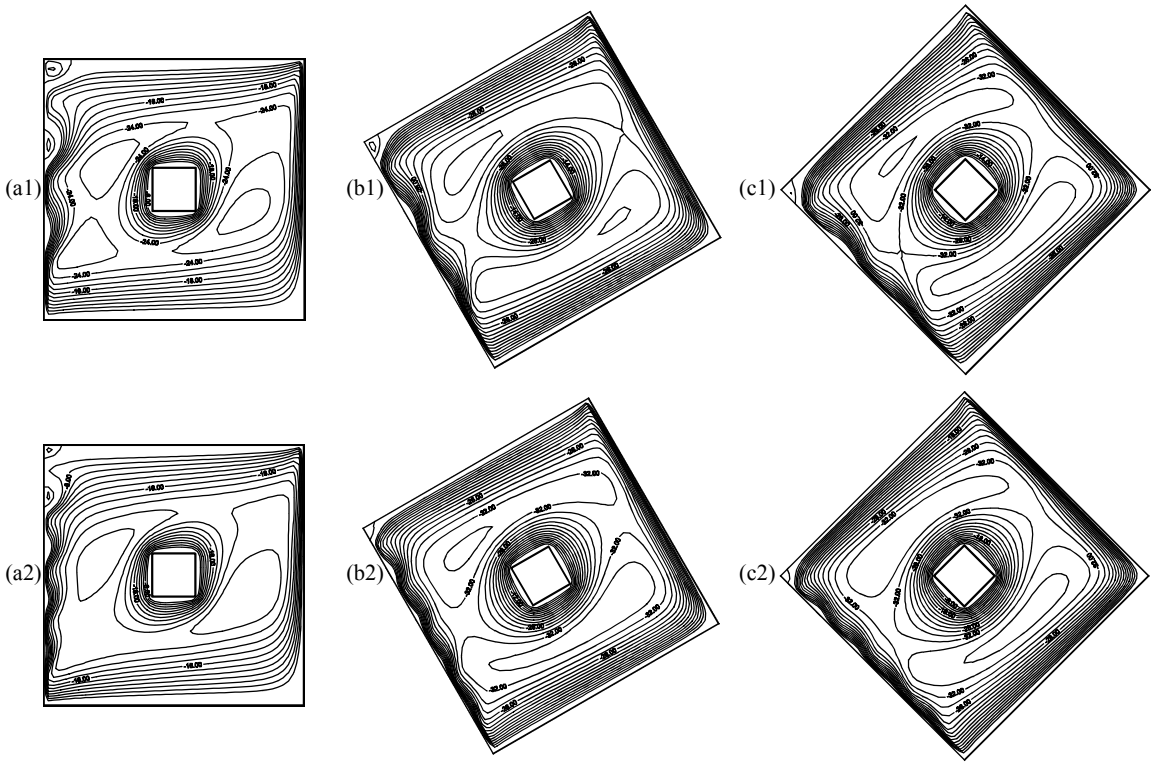

Fig. 7. Streamlines of Flow at Ra= 1000, ε=1 & Dr= 0.15 for a) φ = 0° , b) φ = 30°, c) φ = 45° , and 1) f = 3, 2) f = 5.

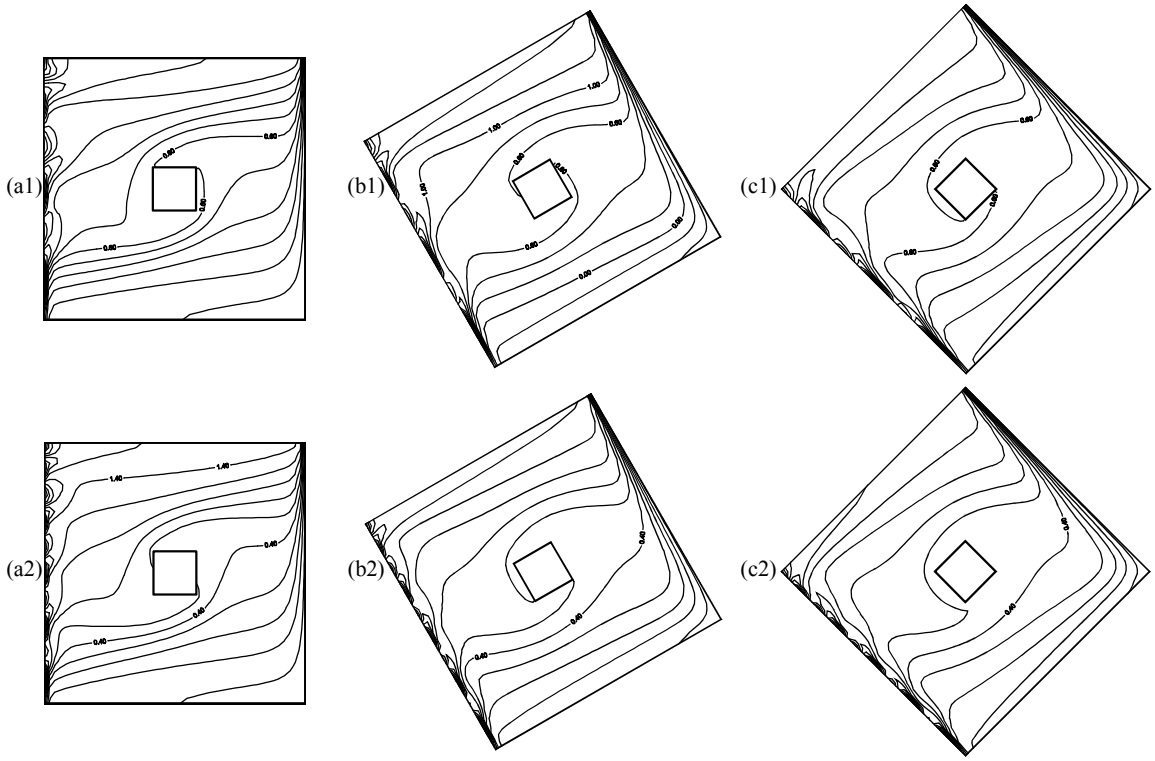

Fig. 8. Isothermal Contours at Ra= 1000, ε=1 & Dr= 0.15 for a) φ = 0° , b) φ = 30° , c) φ = 45° and 1) f = 3, 2) f = 5.

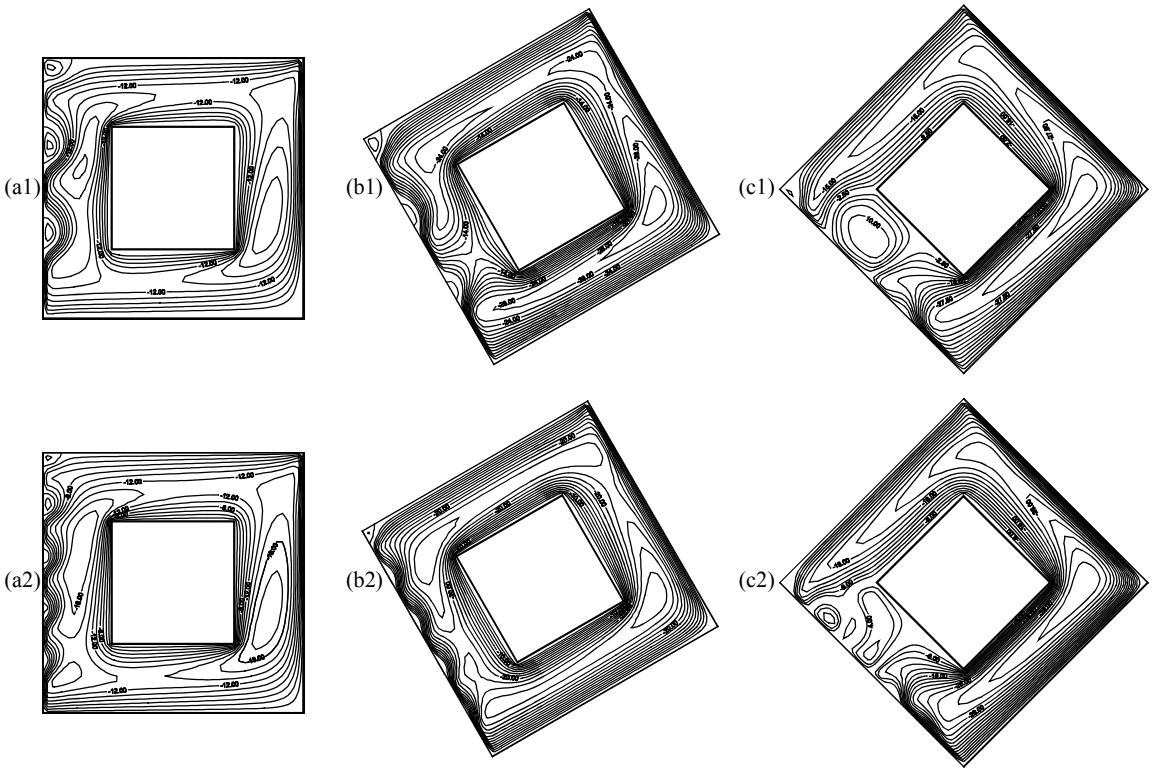

Fig. 9. Streamlines of Flow at Ra= 1000, ε=1 & Dr= 0.45 for a) φ = 0° , b) φ = 30° , c) φ = 45° and 1) f = 3, 2) f = 5.

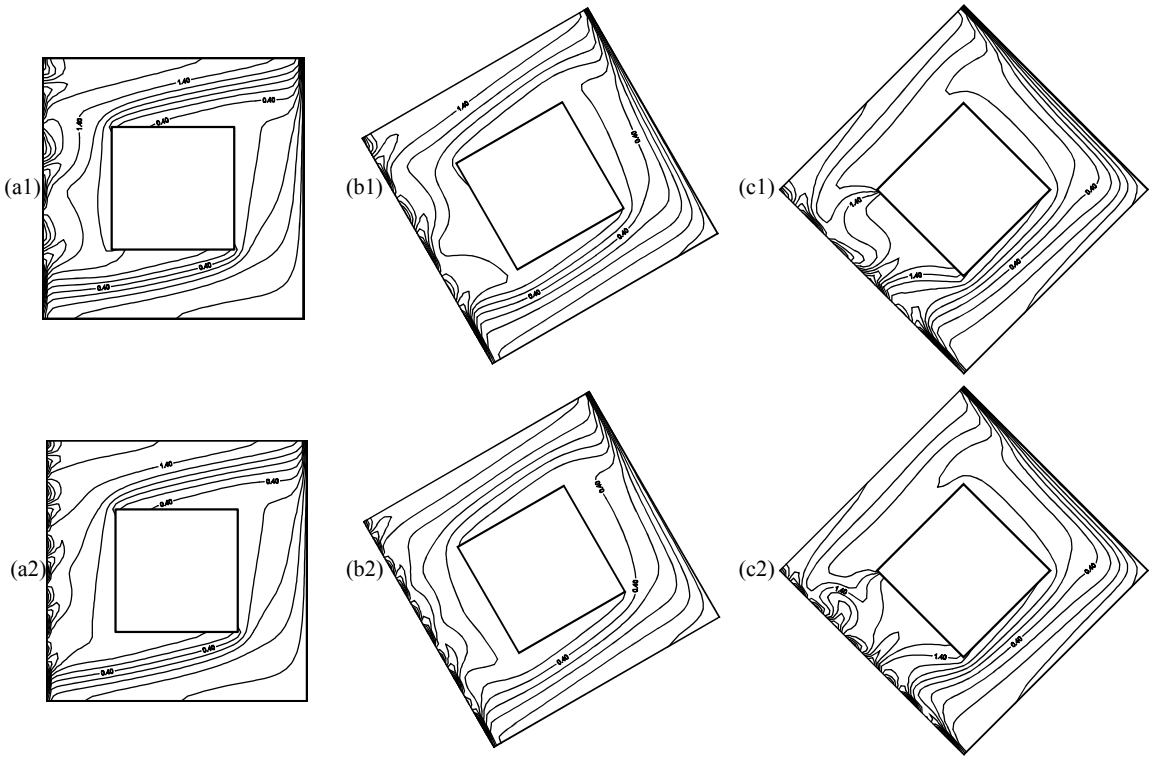

Fig. ١٠. Isothermal Contours at Ra= 1000, ε=1 & Dr= 0.45 for a) φ = 0° , b) φ = 30° , c) φ = 45° and 1) f = 3, 2) f = 5.

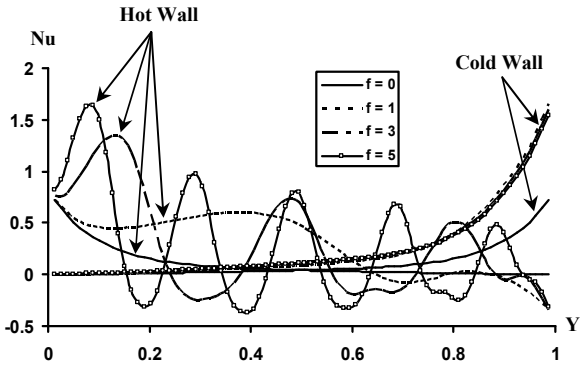

Fig.١١. Distribution of Local Nusselt Number at Ra= 1000, Dr=0.3, ε =0.6, & φ=0

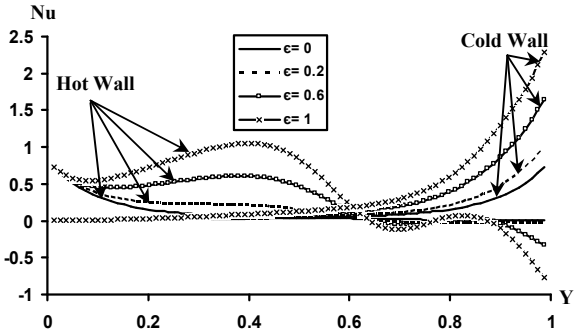

Fig.١٤. Distribution of Local Nusselt Number at Ra= 1000, Dr=0.3, f =1, & φ=0

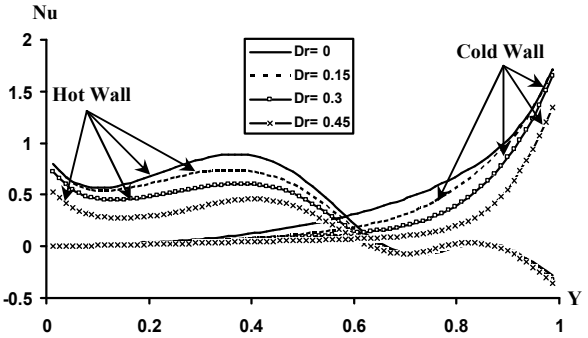

Fig.١٢. Distribution of Local Nusselt Number at Ra= 1000, f = 1, ε =0.6, & φ=0

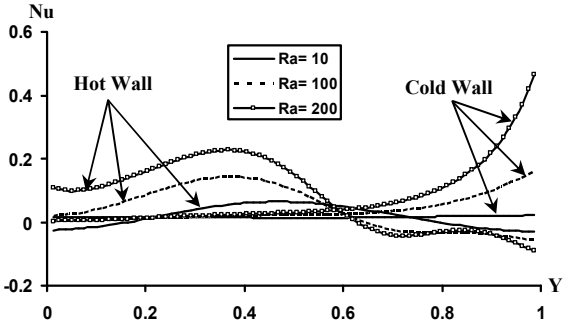

Fig.١٥. Distribution of Local Nusselt Number at Dr=0.3, φ=0, ε =0.6, & f =1

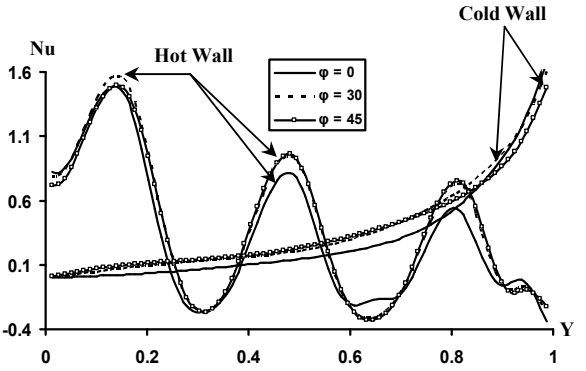

Fig.١3. Distribution of Local Nusselt Number at Ra= 1000, Dr=0.15, ε =0.6, & f =3

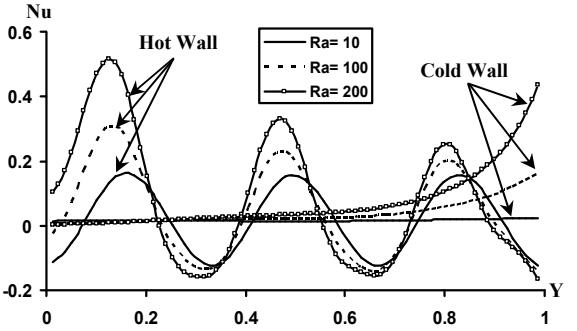

Fig.١٦. Distribution of Local Nusselt Number at Dr=0.3, φ=0, ε =0.6, & f =3

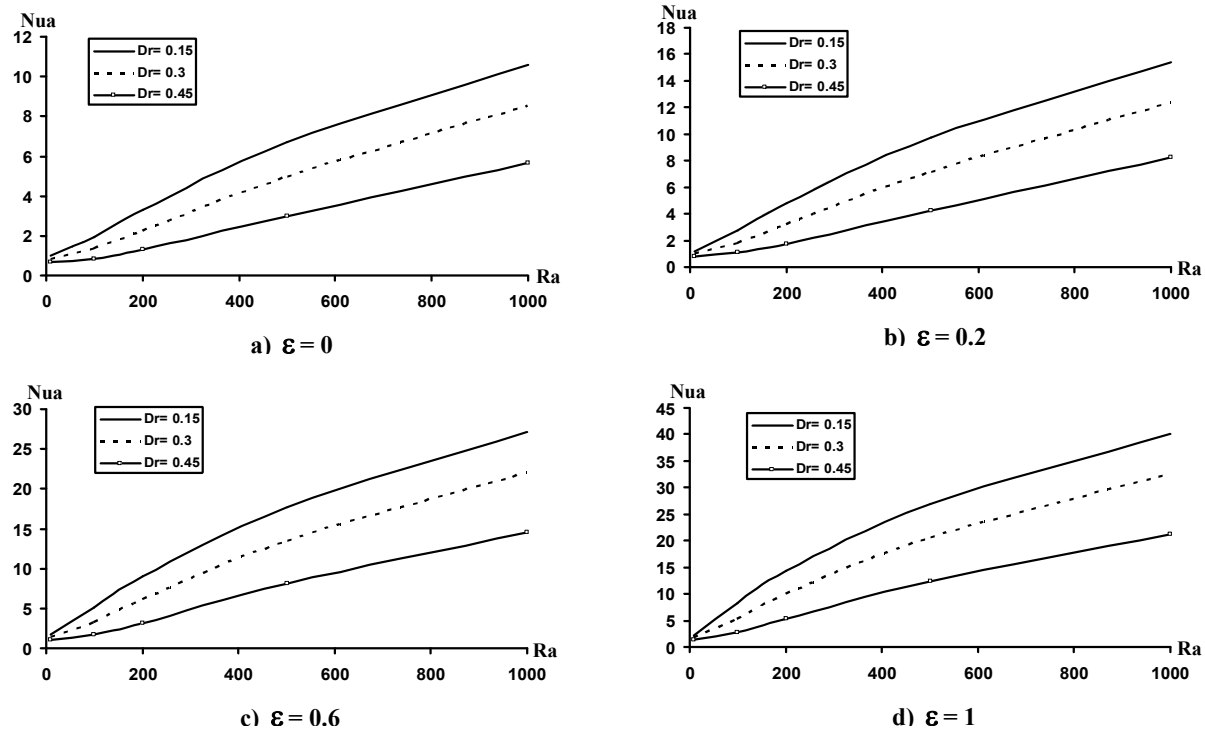

Fig.١7. Variation of Average Nusselt Number on the Hot Wall for Different Values of Rayleigh Number (Ra), Dimension Ratio (Dr), and Amplitude (ε) at φ=0 & f =3.

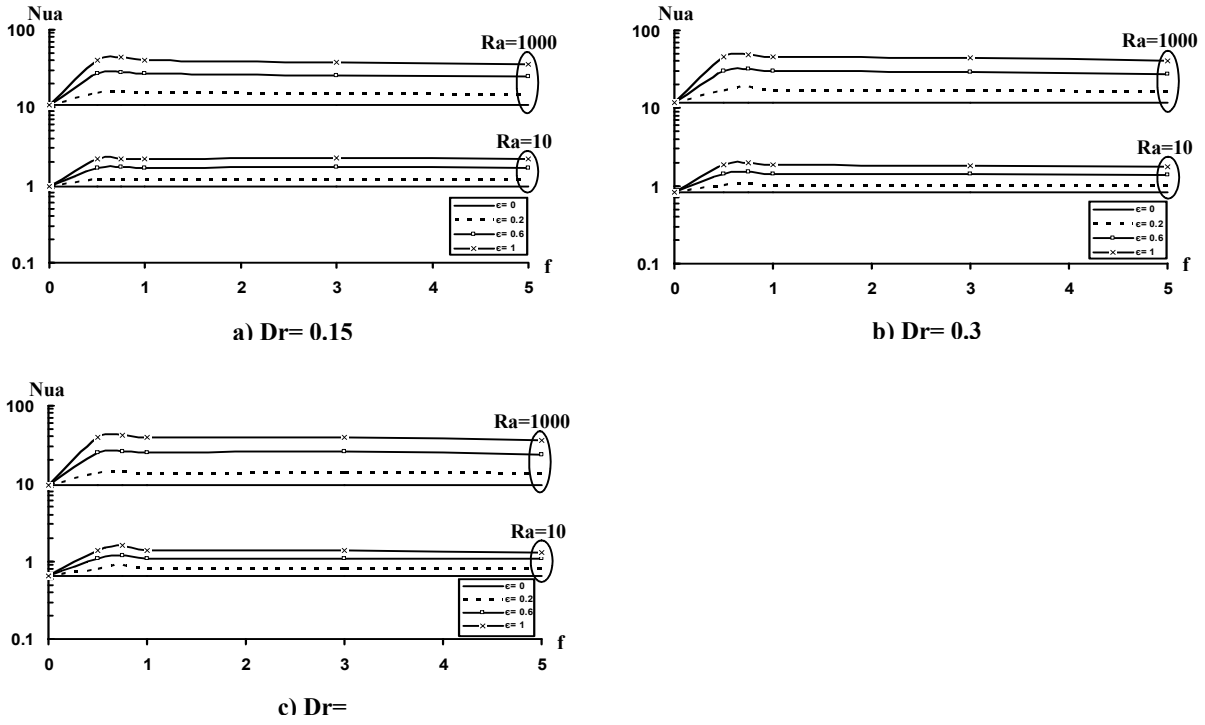

Fig.١٨. Variation of Average Nusselt Number on the Hot Wall for Different Values of Dimension Ratio (Dr), Amplitude (ε), and Wave Number (f) at Ra = 10 & 1000, and φ=30°.

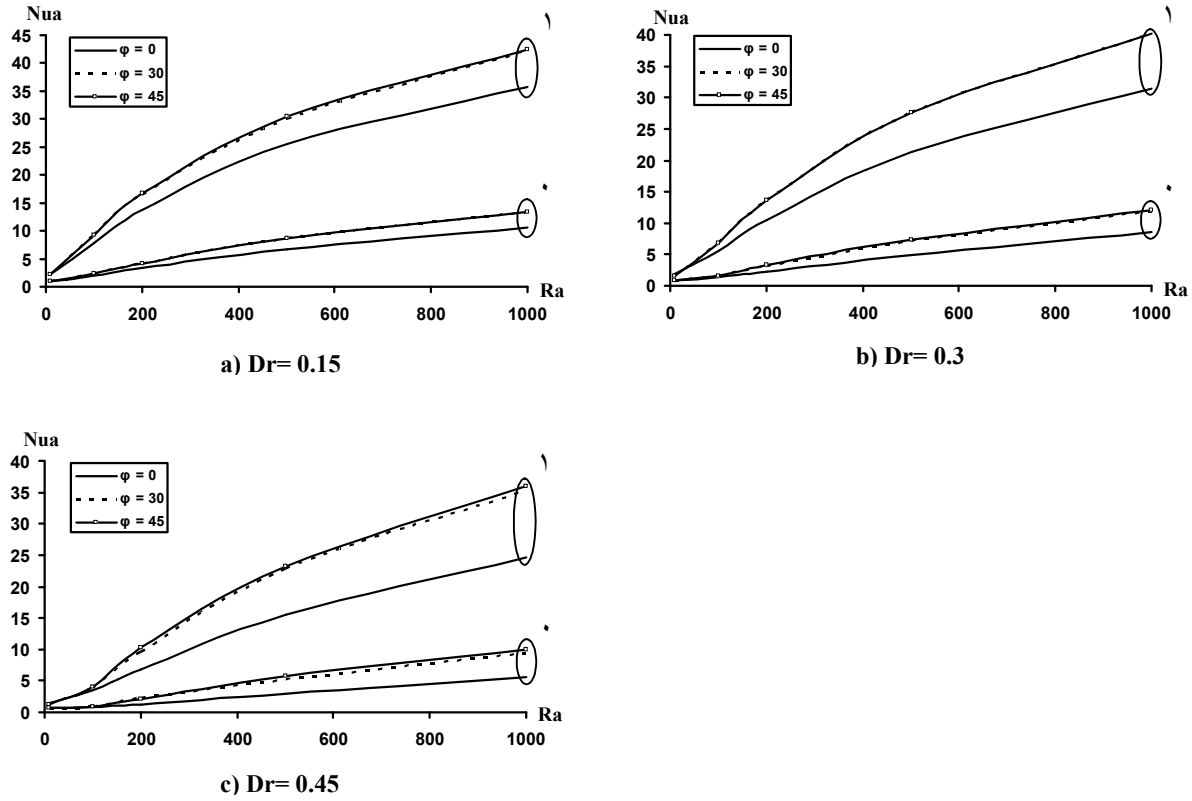

Fig.١٩. Variation of Average Nusselt Number on the Hot Wall for Different Values of Rayleigh Number (Ra), Amplitude (ε), and Dimension Ratio (Dr) at f =5.

Nomenclature

Dr	Dimension ratio, (L_1/L).
g	Gravitational acceleration, (m/s^2).
K	Permeability of the porous medium, (m^2).
f	Wave number of heated side wall temperature (wave frequency).
L	width or height of the outer wall, (m).
L_1	width or height of the inner wall, (m).
n	Total number of grid points.
Nu	Local Nusselt number.
Nu_a	Average Nusselt number.
Ra	Rayleigh number for porous medium.
T	Temperature, (k).
u,v	Velocity components, (m/s).
x,y	Cartesian coordinates, (m).
X,Y	non-dimensional coordinates.

Greek symbols

α	Thermal diffusivity, (m^2/s).
β	Thermal expansion coefficient, (1/k).
ε	Non-dimensional amplitude.
φ	Inclination angle, (degree).
θ	Non-dimensional temperature.
μ	Dynamic viscosity, (kg/m.s).
ρ	Density, (kg/m^3).
ψ	Stream function, (m^2/s).
Ψ	Non-dimensional stream function.

Subscript

c Cold.

h Hot.

7. References

[1] Nield, D. and Bejan, A., "Convection in Porous Media", 2nd edition, Springer, New York, Ny, (1999).

[2] P. Cheng, "Heat Transfer in Geothermal Systems", Adv. Heat Transfer 4 (1978), 1–105.

[3] P.H. Oosthuizen, and H. Patrick, "Natural Convection in an Inclined Square Enclosure Partly Filled with a Porous Medium and with a Partially Heated Wall", HTD 302, American Society of Mechanical Engineers, Heat Transfer Division, (Publication), (1995), 29–42.

[4] P. Nithiarasu, K.N. Seetharamu, and T. Sundararajan, "Numerical Investigation of Buoyancy Driven Flow in a Fluid Saturated non-Darcian Porous Medium", Int. J. Heat Mass Transfer 42 (7) (1998), 1205–1215.

[5] A.M., Al-Amiri, "Analysis of Momentum and Energy Transfer in a Lid Driven Cavity Filled with a Porous Medium", Int. J. Heat Mass Transfer 43 (2000), 3513–3527.

[6] Nawaf H. Saeid, "Natural Convection in a Square Porous Cavity with an Oscillating Wall Temperature", The Arabian Journal for Science and Engineering, Vol. 31, NO. 1B (2005), 35 – 46.

[7] J.P. Caltagirone, and S. Bories, "Solutions and Stability Criteria of Natural Convective Flow in an Inclined Porous Layer", J. Fluid Mech. 155 (6) (1985), 267–287.

[8] P. Vasseur, M.G. Satish, and L. Robillard, "Natural Convection in a Thin Inclined Porous Layer Exposed to a Constant Heat Flux", Int. J. Heat Mass Transfer 30 (3) (1987), 537–549.

[9] M. Sen, P. Vasseur, and L. Robillard, "Multiple Steady States for Unicellular Natural Convection in an Inclined Porous Layer", Int. J. Heat Mass Transfer 30 (10) (1987), 2097–2113.

[10] A.C. Baytas, "Entropy Generation for Natural Convection in an Inclined Porous Cavity", Int. J. Heat Mass Transfer 43 (12) (2000), 2089–2099.

[11] Saeid, N. H. and Mohamed, A., "Periodic Free Convection From a Vertical Plate in a Saturated Porous Medium, non-Equilibrium Model", International Journal of Heat and Mass Transfer, Vol.48. (2006), 3855 - 3863.

[12] Yoo, J.S., "Thermal Convection in a Vertical Porous Slot with Spatially Periodic Boundary Temperature", International Journal of heat and mass transfer, Vol. 46, issue 2, (2003), 381-384.

[13] Robert W., "Numerical Marching Techniques for Fluid Flow with Heat Transfer", Lewis Research Center Cleveland, Ohio and Carnegie – Mellon University Pittsburgh, Pennsylvania.

[14] Najdat N. A., "Laminar Flow Separation in Constructed Channel", Ph.D. Thesis, Michigan State University, 1987.

[15] John D. Anderson, "Computational Fluid Dynamics', International Editions 1995 By McGraw – Hill.

[16] Chan, B. K., Ivey, C. M., and Barry, J. M., "Natural Convection in Enclosed Porous Medium with Rectangular Boundaries", Journal of heat transfer, vol.2, (1970), 21-27.

[17] Burns, P. J., Chow, L. C., and Tien, C. L., "Convection in Vertical Slot filled with Porous Insulation", Int. Journal of heat mass transfer, vol.20, (1974), 919-926.

[18] Bejan, A., and Tien, C., "Natural Convection in a Horizontal Porous Medium Subjected to an End-to-End Temperature Difference", Journal of heat transfer, vol.100, (1978), 191-198.

انتقال الحرارة بالحمل الحر في تجويف مائل بين فجوتين مربعتين متحدتين المراكز ممتلئ بوسط مسامي و مسخن بدرجة حرارة غير منتظمة

نبيل محمد جاسم
قسم الهندسة الميكانيكية/ كلية الهندسة/ جامعة الكوفة
البريد الالكتروني: nabeelalzurfi@yahoo.com

الخلاصة

نعرض في هذا البحث دراسة عددية لتدفق الحمل الحر المستقر في بعدين داخل تجويف مائل بين فجوتين مربعتين متحدتين المراكز ممتلئ بوسط مسامي حيث تكون الجدران الخارجية الجانبية مسخنة بدرجة حرارة مختلفة بينما تكون جميع الجدران الأخرى معزولة. تم استخدام نموذج دارسي للوسط المسامي وقد افترض إن المائع هو مائع بوسين المعياري. الحل العددي للمعادلات أنجز بواسطة طريقة الفروقات المحددة و تطبيق طريقة (كاوس – سيدل) مع استخدام طريقة تحت التراخي. تم تمثيل النتائج العددية بدلالة خطوط الانسياب و درجات الحرارة بالاعتماد على قيم مختلفة لعدد رايلي (من ١٠ إلى ١٠٠٠) , نسبة البعد (من 0.15 إلى 0.45), و زاوية الميل (من 0^{o} إلى 45^{o}). كما تم دراسة تأثير كل من سعة الموجة (من ٠ إلى ١) و عدد الموجات (من ٠ إلى ٥) لدرجة الحرارة المتغيرة للجدار الجانبي الخارجي المسخن على انتقال الحرارة. النتائج بينت تأثير المعاملات السابقة (Ra, Dr, φ ε , and f) على خطوط الجريان و درجة الحرارة. كما بينت النتائج إن عدد نسلت هو دالة قوية من عدد رايلي زاوية الميل نسبة البعد دور التغير في درجة الحرارة. وتتمركز القيمة القصوى لمعدل عدد نسلت عندما تكون قيمة نسبة البعد مساوية إلى (0.15), و زاوية الميل (40.1^{o}) و عندما تكون سعة و عدد الموجات مساوية إلى (١ و ٠.٧٥) لقيمة عدد رايلي (١٠٠٠).